# MEASUREMENT AND ANALYSIS OF HIGH ENERGY GAMMA RAY AND NEUTRON IN MOX FUEL LATTICES FOR SUBCRITICALITY ESTIMATION

**Yashushi NAUCHI*, Takanori KAMEYAMA, Tetsuo MATSUMURA**
Central Research Institute of Electric Power Industry, JAPAN
2-11-1, Iwado Kita, Komae-shi, Tokyo 201-8511 JAPAN
nauchi@criepi.denken.or.jp

**Takenori SUZAKI, Yoshinori MIYOSHI**
Japan Atomic Energy Research Institute
Tokai-Mura, Naka-Gun, Ibaraki-Ken 319-1195, JAPAN

## ABSTRACT

Subcritical MOX fuel lattices were mocked up in tank type core of TCA facility at JAERI. High energy (>3MeV) gamma rays and neutrons originated in the radioactive decay of plutonium and americium nuclides were measured at outside of the lattices in order to investigate the relation of mass of plutonium, effective multiplication factor $k_{eff}$ and those radiations. The transport and multiplication of neutrons and gamma rays in the lattices were calculated with the MCNP-4C code. Neutron yields and spectra from spontaneous fission and ($\alpha$,n) reactions of actinides were obtained with the SOURCES4A code, and yield data of decay gamma rays were obtained with the ORIGEN-2 code. These numerical analyses reproduced the measured data within 5.7% for neutrons and within 5.8% for gamma rays.

The analyses provided the total yield of neutrons and high energy gamma rays in the systems. The total yield ratio of high energy gamma rays to neutrons were compared with the effective multiplication factor $k_{eff}$ calculated with the MCNP-4C code. The ratio was found to have linear relation to the $k_{eff}$. The relation is caused by the fact that the neutron multiplication in chain reaction can be approximated by $1/(1-k_{eff})$ and that the yield ratio in radioactive decay differs from that in neutron induced reaction.

## 1. INTRODUCTION

The strategy has been launched to utilize recycled plutonium in commercial light water reactors in the form of plutonium – uranium mixed oxide (MOX) fuel by Japanese utilities. In the stage of regular use, MOX fuel assemblies are transported to power sites and stored in light water pools prior to loading in a core. In the MOX fuel storage, much caution should be paid to neutron multiplication and sequential emission of gamma rays for criticality and radiation shielding, because MOX fuels radiate more neutrons and gamma rays than UOX fuels. Accordingly, transport of gamma rays and neutrons generated in the fuel assemblies should be well investigated in relation to effective multiplication factor $k_{eff}$ and radiation source intensity.

For the purpose above, subcritical MOX fuel lattices were mocked up in the tank – type critical assembly (TCA) facility at Japan Atomic Energy Research Institute (JAERI). High energy (>3 MeV) gamma ray and neutron flux were measured in the outer region of the lattices in order to investigate the relation of plutonium mass, $k_{eff}$ and those radiations flux.

In this work, source intensity and transport of those radiations in the lattices were analyzed with numerical calculations. The accuracy of the calculations was confirmed by comparing with the measured flux data. Relation between $k_{eff}$ and total yield ratio of high energy gamma rays to neutrons was deduced clearly, which would be useful to approximate the $k_{eff}$ of the MOX fuel lattices in deep subcritical state.

## 2. EXPERIMENTS

The experiment was carried out in the TCA facility at JAERI [1]. The TCA facility consists essentially of a core tank (1.83m in diameter and 2.08m in height), grid plates and fuel rods. Fuel rods are inserted vertically to the grids of square lattice. The lattice pitch is 1.956cm. The moderator is pure light water. Reactivity is adjusted by raising the water level with feeding pump attached to the bottom of the core tank. Four kinds of enrichment (1.1, 2.0, 3.4 and 4.6 %-w/o (Pu+Am)/(Pu+Am+U)) of plutonium – natural uranium mixed oxide fuel were utilized. The isotopic composition of plutonium is shown in Table 1. The density of the fuel was 6.6g $cm^{-3}$ and diameter of it was 1.07cm. The cladding was Zircaloy-2 tube and its outer diameter was 1.224cm. The length of fuel filled in rods was 70.6cm. In addition to MOX fuels, UOX fuel rods of 2.6%-w/o $^{235}U$ enrichment with aluminum cladding were used. The effective length of the rods was 144.2cm. Four kinds of MOX lattices named P-4, P-6, P-8 and P-10 were mocked up at the center of the core tank as shown in Figure 1. Fuels of higher plutonium content were loaded in central part of the lattices, and those of lower plutonium content were loaded in peripheral part. In addition, a combined MOX – UOX lattice (U16-P10) in which the UOX fuel rods surrounded the P-10 lattice were constructed to expand the range of $k_{eff}$. The lowest level of both the MOX and UOX fuels was set on the same plane.

Table 1. The isotopic composition of plutonium and americium in MOX fuels

| | $^{238}Pu$ | $^{239}Pu$ | $^{240}Pu$ | $^{241}Pu$ | $^{242}Pu$ | $^{241}Am$ |
|---|---|---|---|---|---|---|
| Weight Ratio | 0.7 | 65 | 21.5 | 3 | 2.9 | 6.9 |

Each lattice was immersed in pure water. The water level was 66.2cm from the bottom of the fuels. In the fuels, spontaneous fission and $\alpha$ decay occur followed by sequential $\gamma$ decay and ($\alpha$, n) reactions. Besides, those neutrons from the spontaneous fission and the ($\alpha$, n) reactions induce chain reaction which radiate secondary neutrons and gamma rays. Among those radiations, high energy gamma rays (>3MeV) were measured in water region surrounding each lattice by a NaI(Tl) counter located 60cm from the center of the lattice. By setting the lowest energy of detecting to 3MeV, gamma rays of 2.223MeV from H(n,gamma) reactions were discriminated. Thermal neutron flux was measured in the water region by a cylindrical shaped $^{10}B$ proportional counter located 45cm from the center of each lattice. The distance from each lattice to the counters was determined so that the counters did not influence to the neutron multiplication. Distribution of thermal neutron flux was also measured along the bold line indicated in Figure 1 by a micro fission counter containing $^{235}U$. The counter was traversed on the guide made of acryl that was temporarily set between the fuel rods. The vertical position of the traversing was 45cm from the bottom of fuel.

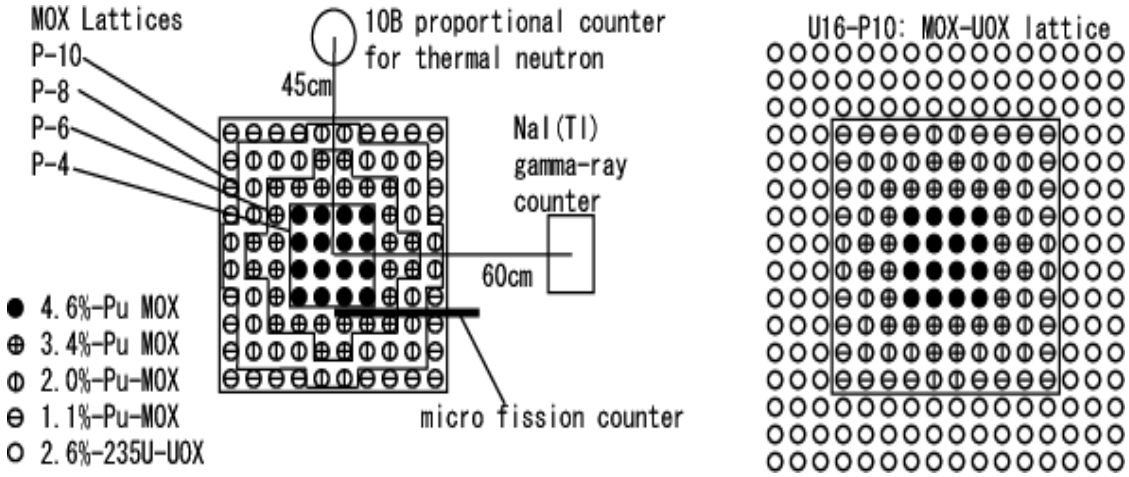


Figure 1. Horizontal schematic view of 5 types of subcritical MOX lattices and counters.

## 3. NUMERICAL ANALYSIS OF RADIATIONS

### 3.1 ANALYSIS OF NEUTRON TRANSPORT

Neutron transport in these subcritical systems is essential to evaluate the yield of gamma rays from neutron chain reaction, thus the neutron flux were calculated at first.

In subcritical systems, the neutron flux is determined by the neutron yield from decay of actinides and the transport efficiency. The neutron source consists of two components, spontaneous fission and ($\alpha$,n) reactions. Neutron yield data or yield calculation codes have been reported for both reactions, but discrepancies have been found among them [2][3]. In the present work, the SOURCES4A code [4] developed in Los Alamos National Laboratory (LANL) was employed. With the code, the absolute neutron spectra of both reactions were calculated for each fuel rod considering the isotopic composition and pellet density.

For the calculation of the transport efficiency, the continuous energy Monte Carlo transport code MCNP-4C developed in LANL [5] was employed. The flux was calculated as fixed source problems, modeling the total length of each fuel rod and considering pin - wised Pu content for neutron source intensity. The $^{10}$B counter located in water region outside lattices was treated as water. Neutron spectrum at the counter was tallied in a water sphere of 5cm in diameter. The $^{10}$B(n,$\alpha$) reaction rate per source neutron was obtained by the product of the calculated neutron spectra and the reaction cross section. As the same way, reaction rate in the fission counter at inside of each lattice was tallied in rectangular volume (6.6cm height in axial direction, 2mm width between fuel pellets and 0.978cm width on the axis of the guide) neglecting the structure of the fission counter and the guide. ENDF60 library included in DLC-200 data set [6] was applied as the point – wised nuclear data set for the calculations since it accommodates the gamma ray yield data in neutron induced reactions for all nuclides, except for zirconium and $^{238}$Pu. As for the zirconium, the data from FSXJ3R2 [7] library were supplemented. Additionally, TMCCS library also included in the DLC-200 was used for inelastic scattering of thermal neutrons on $H_2O$ molecular.

Calculated $^{10}B(n,\alpha)$ reaction rates are compared with the measured data in Figure 2. The reaction rate increased as neutron multiplication factor increased with the lattice size. Calculations reproduced the measured reaction rates within the accuracy of 5.7%. Calculated reaction rate of $^{235}U$ are shown in Figure 3 in comparison with the measured count rates. In spite of neglecting the perturbation from the acryl guide and fission counter, calculated thermal neutron flux was agreed well with that by measurement although statistical fluctuation was seen in measured data. As the results, the calculation method of neutron flux with the SOURCES4A code and the MCNP-4C code is valid for these subcritical MOX experiments.

The effective multiplication factor $k_{eff}$ was calculated for the each lattice with the MCNP-4C code as an eigenvalue problem and shown in Table 2. The lattices mocked up in the experiments covered wide range of the $k_{eff}$ from 0.35 to 0.9.

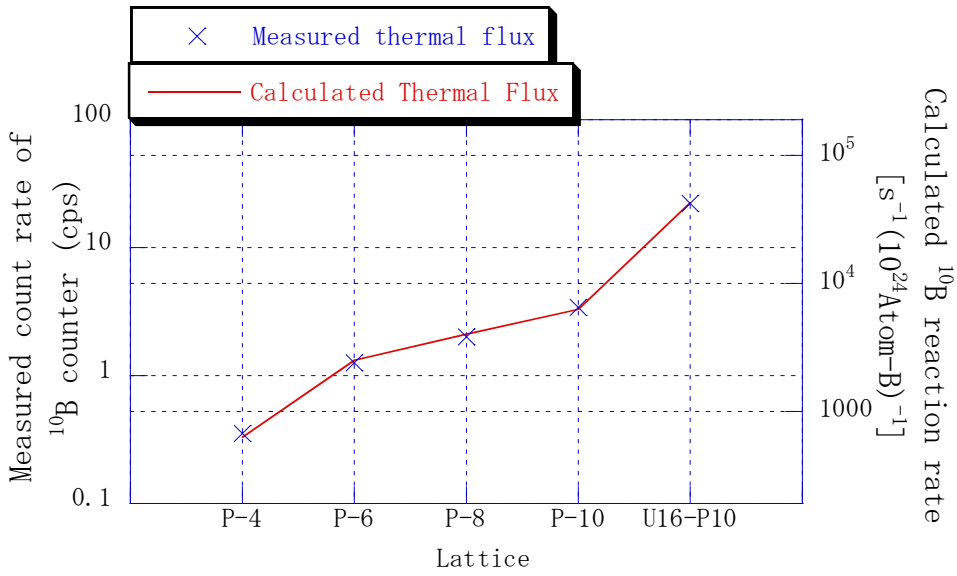


Figure 2. Comparison of calculated $^{10}B(n,a)$ reaction rate in surrounding water region with the count rate of $^{10}B$ proportional counter.

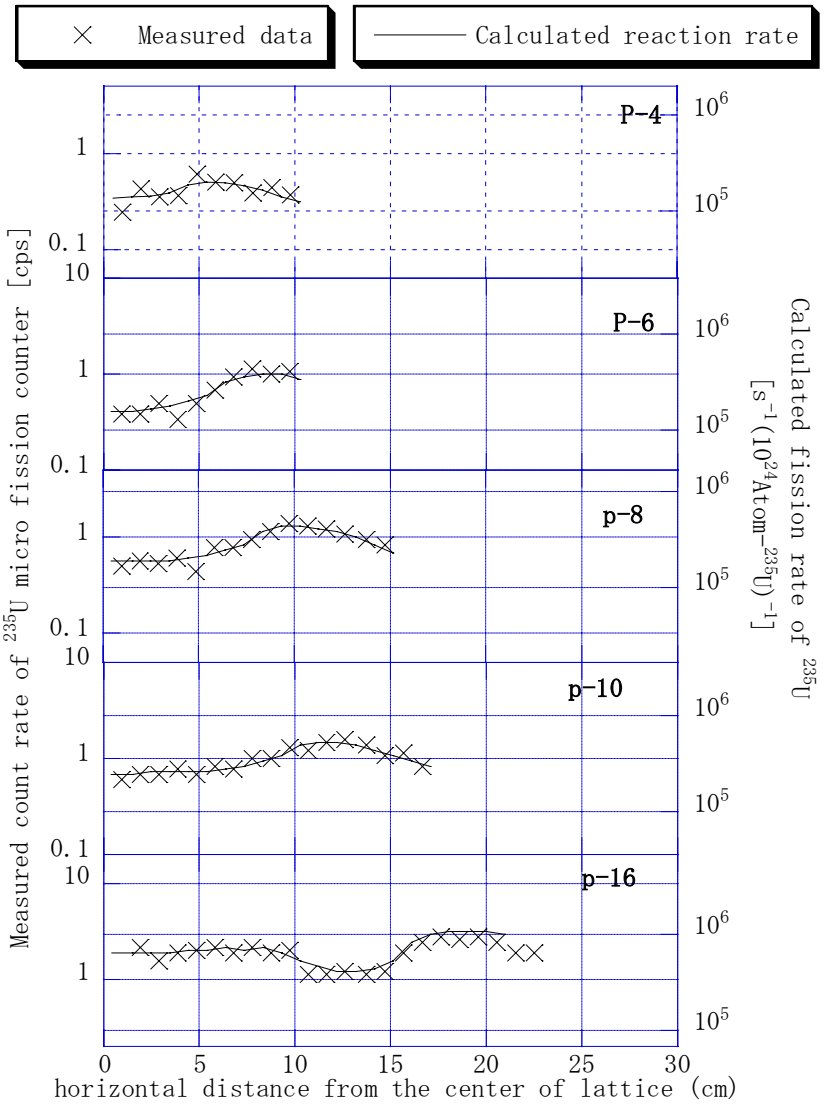


Figure 3. Comparison of calculated thermal flux distribution with the measured count rate of micro fission counter containing $^{235}U$.

Table 2. The effective multiplication factor $k_{eff}$ calculated for each lattice

| Lattice | P-4 | P-6 | P-8 | P-10 | U16-P10 |
|---|---|---|---|---|---|
| $k_{eff}$ | 0.362 | 0.530 | 0.584 | 0.650 | 0.892 |

## 3.2 ANALYSIS OF GAMMA RAY TRANSPORT

Gamma ray flux in the subcritical systems here consists of primary and secondary components. The primary component is from radioactive decay, and secondary one is from neutron induced reaction. The gamma ray flux $\psi$ at the counter is denoted by decay gamma ray yield: $G_0$, transport efficiency of

the primary gamma ray to the counter: $\varepsilon_1$, neutron source intensity $S_0$ and neutron – photon coupled transport efficiency to the counter: $\varepsilon_{n\text{-}g}$.

$$\psi = G_0\varepsilon_1 + S_0\varepsilon_{n-g} \quad (1)$$

The absolute source spectra of the primary gamma rays were calculated with the ORIGEN-2 code [2] that is widely used for calculation of buildup and decay of radioactive materials. With the code, the absolute decay gamma ray spectra dG/dE of 18 energy groups were obtained for each fuel rod. Among them, the first 4 group spectra of energy range 11-8, 8-6, 6-4, 4-3MeV were utilized in the calculation. As for the source of secondary gamma rays, the calculated neutron spectra with the SOURCES4A code were adopted

Both $\varepsilon_1$ and $\varepsilon_{n\text{-}g}$ were calculated with the MCNP-4C code, the former was calculated by photon transport mode and the latter was calculated by neutron – photon coupled transport mode. Gamma rays of higher energy than 3MeV were scored with a point detector estimation tally at the counter position. In the efficiency calculation, $^{241}$Am in MOX fuels was not considered since the photon transport cross section data have not been available here, although $^{241}$Am was considered in the assessment of neutron source intensity because of its large decay constant of α decay. The reactivity effect of $^{241}$Am was calculated to be within 4% for the lattices. Besides, in the use of ENDF60 library, the photon creation data of $^{238}$Pu are also lacked, although the neutron cross sections were considered.

In Figure 4, calculated gamma ray flux is compared with the measured count rate. Primary gamma ray flux increased as the lattice expanded from P-4 lattice to P-10 lattice, but decreased in the U16-P10 lattice. The cause of decrease is that the 2.6%-$^{235}$U-UOX rods emitted much fewer gamma rays than MOX fuel rods and that they only shielded the gamma rays from inner P-10 lattice. Whereas, secondary gamma ray flux monotonously increased with lattice size, and its ratio to the total one exceeded 98% in U16-P10 lattice due to neutron multiplication effect. The calculated total gamma ray flux reproduced the measured flux within accuracy of 5.8%. This accuracy as well as that of neutron flux assures the validity of the calculation methods adopted here.

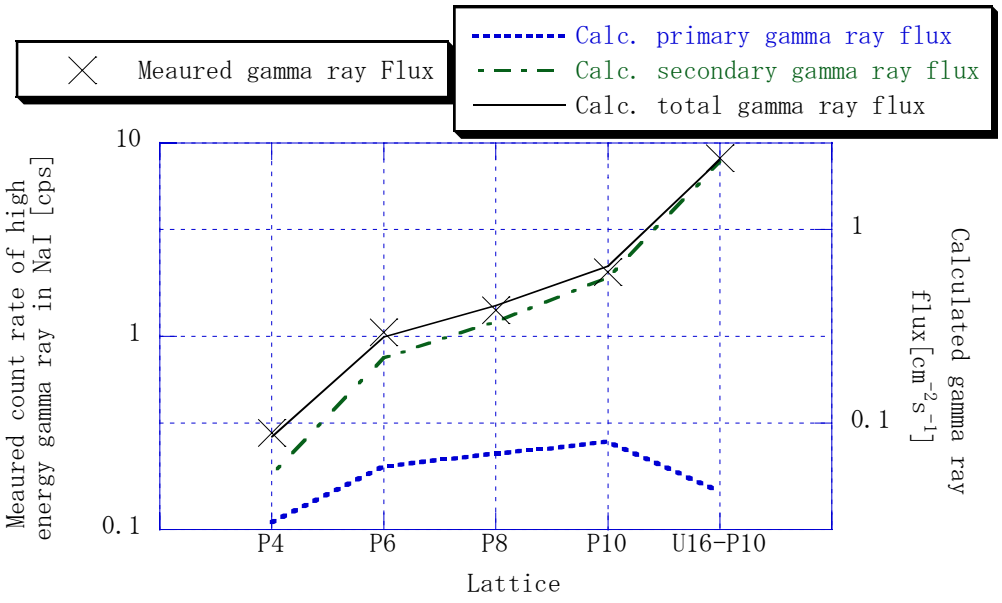


Figure 4. Comparison of the calculated high energy gamma ray flux to the measured count rate on the NaI(Tl) counter.

## 4. YIELD RATIO OF GAMMA RAYS TO NEUTRONS

In the analysis of neutron and gamma ray flux, information was obtained about the neutron multiplication, gamma ray production rate, and transport of both neutrons and gamma rays in the lattices. The total yield of neutrons was obtained by summing up the source intensity with the SOURCES4A code and neutron multiplication with the MCNP-4C code. The total yield of high energy (>3MeV) gamma rays was obtained by summing up the source intensity of the primary gamma rays with the ORIGEN-2 code and the secondary yield with the MCNP-4C code. Here, the total yield ratio of gamma rays to neutrons: (g/n) was correlated with the effective multiplication factor $k_{eff}$ as shown in Figure 5. It is observed that the (g/n) ratio is linearly corresponding to the $k_{eff}$ .

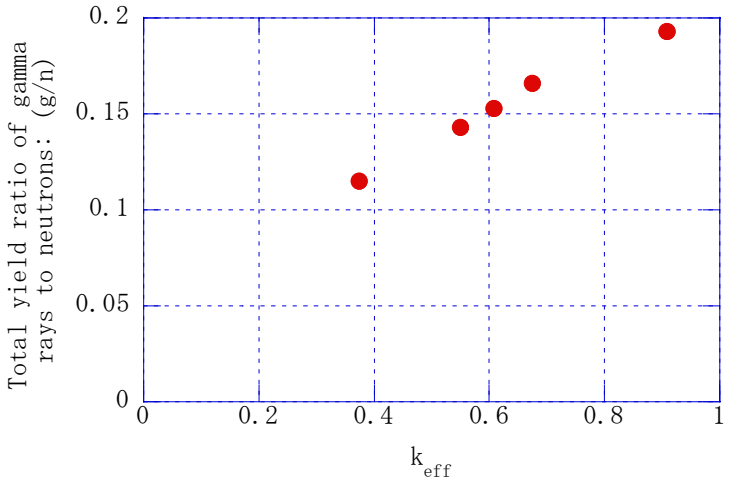


Figure 5. Total yield ratio of high energy gamma rays to neutrons as function of $k_{eff}$.

Generally, total neutron yield S in a subcritical system ($k_{eff} < 1$) has relation to the neutron source intensity $S_0$ defined by the following equations provided that the source distribution is identical in space and energy to those obtained from the solution of an eigenvalue problem.

$$S \approx \frac{S_0}{1-k_{eff}} = S_0 + \frac{k_{eff}}{1-k_{eff}} S_0 \qquad (2)$$

The second term of right hand denotes the yield of secondary neutrons from the chain reaction. In Table 3, the total neutron yield and the quantity of $S_0/(1-k_{eff})$ are tabulated. Although there were differences in the source distribution, the equation (2) was valid within 7.5% accuracy for the 5 lattices.

Table 3. Comparison of total neutron yield and the quantity of source intensity divided by subcriticality: $S_0/(1-k_{eff})$

| | P-4 | P-6 | P-8 | P-10 | U16-P10 |
|---|---|---|---|---|---|
| Total Neutron Yield:S [$s^{-1}$] | 3.279E+05 | 1.004E+06 | 1.425E+06 | 2.126E+06 | 8.839E+06 |
| $S_0/(1-k_{eff})$ [$s^{-1}$] | 3.463E+05 | 1.082E+06 | 1.543E+06 | 2.296E+06 | 8.250E+06 |

In the condition, the total yield of gamma rays: G is expressed as follows using the yield ratio of gamma rays to neutrons in radioactive decay: $(g/n)_{primary}$ and that in neutron induced reaction: $(g/n)_{secondary}$.

$$G \approx G_0 + \frac{k_{eff}}{1-k_{eff}} S_0 \left(\frac{g}{n}\right)_{secondary} = \frac{S_0}{1-k_{eff}} \left[ \left(1-k_{eff}\right)\left(\frac{g}{n}\right)_{primary} + k_{eff}\left(\frac{g}{n}\right)_{secondary} \right] \quad (3)$$

In Table 4, the $(g/n)_{primary}$, the $(g/n)_{secondary}$ and the total (g/n) are tabulated. It is found that the $(g/n)_{primary}$ and the $(g/n)_{secondary}$ are almost constant for lattices, and both values are different. Owing to the difference and the condition of equation (2), the (g/n) value varies linearly to the $k_{eff}$ as follows.

$$\left(\frac{g}{n}\right) = \frac{G}{S} \approx \left[ \left(1-k_{eff}\right)\left(\frac{g}{n}\right)_{primary} + k_{eff}\left(\frac{g}{n}\right)_{secondary} \right] \quad (4)$$

Table 4. The yield ratios of high energy gamma rays to neutrons of radioactive decay and neutron induced reaction calculated for each lattice

| $k_{eff}$ | 0.374 | 0.549 | 0.607 | 0.675 | 0.909 |
|---|---|---|---|---|---|
| $(g/n)_{primary}$ | 0.068 | 0.068 | 0.068 | 0.068 | 0.069 |
| $(g/n)_{secondary}$ | 0.208 | 0.213 | 0.216 | 0.220 | 0.204 |
| (g/n) | 0.115 | 0.143 | 0.153 | 0.166 | 0.193 |

Further studies were done for the yield ratio of gamma rays to neutrons. The $(g/n)_{primary}$ was determined by isotopic composition of fuel rods since all radiations are generated from radioactive decay of actinides. In the chain reaction, almost all of the neutrons (>99.8%) were generated from fission reactions and the secondary gamma rays were also produced mainly in fuel rods as shown in Table5. Thus the ratio $(g/n)_{secondary}$ was determined by reactions of actinides in the fuel rods as well as the $(g/n)_{primary}$. The yields of neutrons and gamma rays from each nuclide in fuel rods were calculated for U16-P10 lattice and tabulated in Table 6. The yields varied with nuclides. $^{240}Pu$ was the major source of primary high energy (>3MeV) gamma rays and was also the principle source of neutrons as well as $^{238}Pu$ and $^{241}Am$, so the composition of those nuclides in the fuel determines the $(g/n)_{primary}$. On the other hand, $^{235}U$ and $^{239}Pu$ fissile nuclides as well as $^{238}U$ mainly radiated secondary gamma rays and fission neutrons, thus they determines the $(g/n)_{secondary}$. Therefore, the total yield ratio of gamma rays to neutrons (g/n) is not only related to $k_{eff}$ mentioned above, but also to the isotopic composition of lattices.

Table 5. Contribution of each component to the total yield of secondary high energy gamma rays in the system

| Lattice | P-4 | P-6 | P-8 | P-10 | U16-P10 |
|---|---|---|---|---|---|
| fuel | 0.952 | 0.949 | 0.946 | 0.941 | 0.935 |
| clad | 0.024 | 0.027 | 0.029 | 0.032 | 0.036 |
| water between fuel rods | 0.003 | 0.003 | 0.004 | 0.004 | 0.004 |

Table 6. High energy gamma ray and neutron yields repartition per isotopes calculated for U16-P10 lattice

| | $^{235}U$ | $^{238}U$ | $^{238}Pu$ | $^{239}Pu$ | $^{240}Pu$ | $^{241}Pu$ | $^{242}Pu$ | $^{241}Am$ |
|---|---|---|---|---|---|---|---|---|
| prinmary gamma ray(/s) | 7.2E-01 | 7.5E+02 | 4.1E+03 | 3.2E+02 | 3.6E+04 | 6.0E-03 | 8.8E+03 | 1.9E+03 |
| neutron(/s) | 4.9E+00 | 2.1E+03 | 1.5E+05 | 3.6E+04 | 2.5E+05 | 5.7E+01 | 4.6E+04 | 2.7E+05 |
| secondary gamma ray(/src) | 9.2E-01 | 3.9E-01 | 0.0E+00 | 6.6E-01 | 3.8E-02 | 2.5E-02 | 1.4E-03 | |
| fission neutron(/src) | 6.5E+00 | 5.2E-01 | 1.0E-03 | 3.4E+00 | 3.9E-02 | 2.0E-01 | 6.5E-04 | |

The (g/n) ratio varies with the lowest energy of gamma ray detection (threshold energy). For various threshold energy, the yield of neutrons and gamma rays were calculated and the quantities of $(g/n)_{secondary}/(g/n)_{primary}$ were deduced for lattices as shown in Table 7. Above 3MeV, the $(g/n)_{secondary}/(g/n)_{primary}$ was almost constant for all lattices and the $(g/n)_{secondary}$ differed largely from the $(g/n)_{primary}$, thus the linear relation of the total yield ratio (g/n) to $k_{eff}$ was preferably assured. For the lower threshold energy below 3MeV, the $(g/n)_{secondary}/(g/n)_{primary}$ was not constant, which is due to the change of $(g/n)_{secondary}$ since the $(g/n)_{primary}$ is determined only by isotopic composition. The variety of the $(g/n)_{secondary}$ is attributed to the H(n,gamma) reactions outside the lattices since the leakage probability of neutrons decreases as the lattice expands horizontally from P-4 lattice to U16-P10 lattice. As the results, the threshold energy of 3MeV is considered to provide the linearity of the total yield ratio (g/n) to $k_{eff}$.

Table 7. The yield ratio of high energy gamma rays to neutrons in decay: $(g/n)_{primary}$ and that in neutron induced reaction: $(g/n)_{secondary}$ with the threshold energy of gamma ray detection

| Threshold | Ratio of $(g/n)_{secondary}/(g/n)_{primary}$ for each lattice | | | | | average | Deviation |
|---|---|---|---|---|---|---|---|
| (MeV) | P-4 | P-6 | P-8 | P-10 | U16-P10 | | (%) |
| 6 | 3.97 | 3.98 | 4.12 | 4.32 | 4.50 | 4.18 | 5.45 |
| 4 | 3.81 | 3.94 | 3.99 | 4.04 | 3.68 | 3.89 | 3.75 |
| 3 | 3.05 | 3.14 | 3.18 | 3.23 | 2.97 | 3.11 | 3.38 |
| 2 | 12.29 | 8.11 | 7.24 | 6.39 | 4.40 | 7.69 | 37.97 |
| 1 | 4.55 | 3.43 | 3.22 | 3.01 | 2.45 | 3.33 | 23.21 |

The linear relation revealed in the present work is considered to be applicable to estimate the $k_{eff}$ of systems in deep subcritical state ($k_{eff}$ = 0.3~0.9) provided that the yield ratio could be measured.

## 5. SUMMARY AND CONCLUSION

Numerical analyses were performed for the flux of thermal neutron and high energy (>3MeV) gamma ray measured in subcritical MOX fuel lattices mocked up in the TCA at JAERI. Transport efficiency of both neutrons and gamma rays were calculated with the MCNP-4C code. The source intensity of neutrons was calculated with the SOURCES4A code and that of high energy gamma rays was done with the ORIGEN-2 code. By selecting the appropriate codes, the analyses reproduced the measured data within 5.8% for both radiations. Through the analysis, it was revealed that the total yield ratio of high energy gamma rays to neutrons shows linear relation to the effective multiplication factor $k_{eff}$. This relation is caused by the fact that the neutron multiplication is approximated by $1/(1-k_{eff})$ and that the yield ratio in radioactive decay differs from that in neutron induced reaction. It was also found that the lowest energy of gamma ray detection must be higher than 3MeV to assure the linear relation.

The linear relation of the total yield ratio to the $k_{eff}$ would be useful for the estimation of $k_{eff}$ of systems in deep subcritical state. Further study will be performed to develop the measurement methods of total yield ratio (g/n) to establish subcriticality monitoring method.

## ACKNOWLEDGEMENTS

The experiments with the MOX fuel rods were performed under a joint research program between JAERI and Japan Nuclear Cycle Development Institute.

## REFERENCES


1. H. Tsuruta, I Kobayashi, T. Suzaki, A. Ohno, K. Murakami, S. Matsuura, "Critical Size of Light Water Moderated $UO_2$ and $PuO_2$-$UO_2$ Lattices," *JAERI Report*, **1254**, (1973).
2. A. G. Croff, "A VERSATILE COMPUTER CODE FOR CALCULATING THE NUCLIDE COMPOSITIONS AND CHARACTERISTICS OF NUCLEAR MATERIALS," *Nucl. Techmnol.,* **62**, pp. 335 (1983).
3. H. Matsunobu, T. Oku, S. Iijima, Y. Naito, F. Masukawa and R. Nakashima, "Data Book for Calculating Neutron Yields from (α,n) Reactions and Spontaneous Fission" (in Japanese), *JAERI*, **1324**, pp.260 (1991).
4. W. B. Wilson, R. T. Perry, W. S. Charlton, T. A. Parish, G. P. Estes, T. H. Brown, E. D. Arthur, M. Bozoian, T. R. England, D. G. Madland, J. E. Stewart, "SOURCES4A: A Code Calculating (α,n) Spontaneous Fission and Delayed Neutron Sources and Spectra," *LA*-**13639** (1999).
5. J. F. Briesmeister et al., "MCNPTM-A General Monte Carlo N-particle transport code," *LA*-, **13709-M**, (2000).
6. J. S. Headricks, S. C. Frankle, J. D. Court, "ENDF-B VI Data for MCNP" *LA*-**12891** (1994).
7. K. Kosako, F. Maekawa, Y. Oyama, Y. Uno and H. Maekawa, "A CONTINUOUS ENERGY CROSS SECTION LIBRARY FOR MCNP BASED ON JENDL-3.2", *JAERI-Data/Code* **94-020**, (1994).